Published in final edited form as:
J Phys Chem A. 2012 July 5; 116(26): 7210–7218. doi:10.1021/jp3039169.

Theoretical and Experimental Studies of the Spin Trapping of Inorganic Radicals by 5,5-Dimethyl-1-Pyrroline *N*-Oxide (DMPO). 3. Sulfur Dioxide, Sulfite and Sulfate Radical Anions

Pedro L. Zamora and **Frederick A. Villamena**[*]
Department of Pharmacology, The Davis Heart and Lung Research Institute and Center for Biomedical EPR Spectroscopy and Imaging, College of Medicine, The Ohio State University, Columbus, Ohio, USA 43210

Abstract

Radical forms of sulfur dioxide (SO_2), sulfite (SO_3^{2-}), sulfate (SO_4^{2-}), and their conjugate acids are known to be generated *in vivo* through various chemical and biochemical pathways. Oxides of sulfur are environmentally pervasive compounds and are associated with a number of health problems. There is growing evidence that their toxicity may be mediated by their radical forms. Electron paramagnetic resonance (EPR) spin trapping using the commonly used spin trap, 5,5-dimethyl-1-pyrroline *N*-oxide (DMPO), has been employed in the detection of $SO_3^{\bullet-}$ and $SO_4^{\bullet-}$. The thermochemistries of $SO_2^{\bullet-}$, $SO_3^{\bullet-}$, $SO_4^{\bullet-}$, and their respective conjugate acids addition to DMPO were predicted using density functional theory (DFT) at the PCM/B3LYP/6-31+G**// B3LYP/6-31G* level. No spin adduct was observed for $SO_2^{\bullet-}$ by EPR but an S-centered adduct was observed for $SO_3^{\bullet-}$ and an O-centered adduct for $SO_4^{\bullet-}$. Determination of adducts as S- or O-centered was made *via* comparison based on qualitative trends of experimental hfcc's with theoretically calculated ones. The thermodynamics of the non-radical addition of SO_3^{2-} and HSO_3^- to DMPO followed by conversion to the corresponding radical adduct *via* the Forrester-Hepburn mechanism was also calculated. Adduct acidities and decomposition pathways were investigated as well, including an EPR experiment using $H_2{}^{17}O$ to determine the site of hydrolysis of O-centered adducts. The mode of radical addition to DMPO is predicted to be governed by several factors, including spin population density, and geometries stabilized by hydrogen bonds. The thermodynamic data supports evidence for the radical addition pathway over the nucleophilic addition mechanism.

Keywords

Sulfur Dioxide Radical Anion; Sulfite Radical Anion; Sulfate Radical Anion; Forrester-Hepburn; EPR; Free Radical; DFT; ROS; Spin Trapping

INTRODUCTION

Sulfur dioxide (SO_2) and its derivatives are environmentally pervasive compounds emitted during combustion of coal, natural gas, and other fossil fuels. A water soluble acid, SO_2 reacts with moisture in the atmosphere or in the lungs to form bisulfite and sulfite (HSO_3^-, SO_3^{2-}) as well as bisulfate and sulfate (HSO_4^-, SO_4^{2-}). Due to their antimicrobial-growth

[*]Correspondence to: Frederick.Villamena@osumc.edu, Fax: (614)-292-688-0999.

Supporting Information Available. Energies, enthalpies, and free energies for all spin traps and their corresponding spin adducts are available as supporting information. This information is available free of charge at http://pubs.acs.org.

properties and antioxidant color-preservation properties, sulfites are also common additives in food, beverages, and pharmaceuticals.[1]

Sulfite, whether ingested or inhaled as SO_2, is known to cause bronchioconstriction in asthmatics,[2] and is toxic to cells of the lung[3] and central nervous system.[4] Sulfite is generated endogenously during the metabolism of the sulfur-containing amino acids cysteine and methionine.[5] Sulfite is detoxified in animal cells by conversion to sulfate *via* the mitochondrial inter-membrane-space enzyme sulfite oxidase.[6] Genetic deficiency of sulfite oxidase in humans results in severe neurological deformity[7] and early death.[8]

There is reason to believe that the toxicity of sulfites is mediated by their radical forms.[9] These radicals have been shown to be photochemically[10] and enzymatically[11,12] generated, or by oxygen-mediated metal-catalyzed oxidation of their respective anions.[13] Reactive oxygen species generated by transition-metal-catalyzed autoxidation of sulfite cause DNA damage[14] and lipid peroxidation.[15] Studies have shown that the toxicity of sulfites in sulfite-oxidase-deficient rats is prevented by treatment with transition metal chelating agents and antioxidants,[15] suggesting a role of sulfur-oxide radicals in toxicity. Once generated *via* the enzymatic actions of prostaglandin synthase,[11] horseradish peroxidase,[11] or in the O_2-rich capillaries of the lungs *via* transition metal catalysis,[13] $SO_3^{\bullet-}$ will react readily with O_2 to form peroxymonosulfate radical anion ($^{-}O_3SOO^{\bullet}$, Equation 1), with peroxymonosulfate radical reacting with sufite to form sulfate and sulfate radical anion (Equation 2).[9]

$$SO_3^{\bullet-} + O_2 \rightarrow {}^{-}O_3O_3SOO^{\bullet} \quad (1)$$

$$^{-}O_3SOO^{\bullet} + SO_3^{2-} \rightarrow SO_4^{2-} + SO_4^{\bullet-} \quad (2)$$

As an extremely strong oxidizing agent, $SO_4^{\bullet-}$ radical chain propagation can be furthered by the tendency of free sulfite to reduce cysteine-cysteine disulfide bonds, forming *S*-sulfocysteine (Equation 3).[16]

$$RSSR' + HSO_3^{-} \rightleftharpoons RSSO_3^{-} + HSR' \quad (3)$$

This equilibrium effectively serves as a reservoir and transporter of HSO_3^{-} to areas of low disulfide concentration. *S*-sulfocysteine can be reduced to yield $SO_3^{\bullet-}$ and initiate the radical chain reaction (Equation 4).

$$RSSO_3^{-} + e^{-} \rightarrow RS^{-} + SO_3^{\bullet-} \quad (4)$$

Investigation into the reactivity of sulfur oxide radical species with probes or with antioxidants is of value in expanding knowledge on the role of sulfites in diseases. In the present study, spin trapping was used to analyze the properties of sulfur oxide radicals (SORs) such as radical anion forms of sulfur dioxide ($SO_2^{\bullet-}$), sulfite ($SO_3^{\bullet-}$), and sulfate ($SO_4^{\bullet-}$). The nitrone, 5,5-dimethyl-1-pyrroline *N*-oxide (DMPO) is the most widely used spin trap due to the ability of its spin adducts to impart discernable EPR spectra from radicals that have very little variations in their structures. For example, the EPR spectrum arising from the addition of $HO^{\bullet}$ or $O_2^{\bullet-}$ to DMPO can be distinguished from one another. While generation of $SO_2^{\bullet-}$ in the presence of spin traps is known to not give a signal,[17] generation of $SO_3^{\bullet-}$ [18,19] and $SO_4^{\bullet-}$ [20] in the presence of spin traps have been shown to give EPR spectra. However, to date, comparative studies on the energetics of spin trapping of SORs using DMPO and structural studies of the possible adducts formed are still lacking.

Controversy still arises in regards to the nature of these SOR adducts and their formation, since for example, Khramstov and co-workers[21,22] have proposed a non-radical pathway for the DMPO$^{\bullet}$-SO_3^- adduct formation *via* nucleophilic addition reaction (Scheme 1).

The importance of spin trapping using nitrone spin traps is twofold; first, spin trapping has been widely employed for the detection of radical species using electron paramagnetic resonance (EPR) spectroscopy,[23] and second, the spin trapping process can yield chemistries[24–31] that are relevant toward the understanding of the antioxidant properties of nitrones.[32,33]

In this work, the relative energetics of SOR additions to DMPO were explored and structural studies of adducts were theoretically performed to address a lack of information in the literature; these studies would otherwise be difficult to experimentally pursue due to the poor yield and instability of the spin adducts.

EXPERIMENTAL METHODS

General Computational Methods

For the addition of each radical species ($SO_2^{\bullet-}$, $HSO_2^{\bullet}$, $SO_3^{\bullet-}$, $HSO_3^{\bullet}$, $SO_4^{\bullet-}$, and $HSO_4^{\bullet}$) to DMPO and for the nucleophilic addition of each non-radical anion (SO_3^{2-}, HSO_3^-), two products were theoretically calculated; an S-centered adduct and an O-centered adduct. Density functional theory[34,35] was applied in this study to determine the optimized geometry, vibrational frequencies, and single-point energy of all stationary points.[36–39] The effect of solvation on the gaseous phase calculations was also investigated using the polarizable continuum model (PCM).[40–44] All calculations were performed using Gaussian 09[45] at the Ohio Supercomputer Center. Single-point energies were obtained at the B3LYP/6-31+G** level based on the optimized B3LYP/6-31G* geometries, and the B3LYP/6-31+G**//B3LYP/6-31G* wave functions were used for Natural Population Analyses (NPA).[46] These basis set calculations used the standard six Cartesian d functions. Vibrational frequency analyses (B3LYP/6-31G*) for each of the stationary points for DMPO and its spin adducts yielded only real vibrational frequencies. A scaling factor of 0.9806 was used for the zero-point vibrational energy (ZPE) corrections with the B3LYP/6-31G* and the B3LYP/6-311+G* levels of theory.[47] Spin contamination for all of the stationary point of the radical structures was negligible, i.e., $0.75 < \langle S^2 \rangle < 0.77$ except for the S-centered DMPO$^{\bullet}$-SO_4 adduct that has $S^2 = 1.72$.

Calculation of Isotropic Hyperfine Coupling Constants (hfcc)

The prediction of hfcc of the nitrogen atom in simple nitroxides was demonstrated in several benchmark studies.[43,48–50] Based on these previous studies, we employed similar models in the prediction of hfcc's of the nitrogen, β-hydrogen and γ-hydrogens of the various sulfur oxide radical (*i.e.,* $SO_2^{\bullet-}$, $SO_3^{\bullet-}$, $SO_4^{\bullet-}$, and their respective conjugate acids) adducts of DMPO. A discussion of the comparative study of calculated hfcc for DMPO-O_2H optimized at the B3LYP density functional and basis sets, 6-31+G**, 6-31G*, EPR-II and EPR-III,[51] and the core-valence correlation-consistent cc-pCVDZ[52] in the gas and aqueous phases can be found in pages S13–S18 of Supplementary Material Section of our previous paper.[53] In the same paper,[53] the hybrid PBE0 functional and EPR-II basis set was found[50] to yield accurate a_N values in simple nitroxides and was also employed in the calculation of hfcc for DMPO-O_2H. Although the levels of theory mentioned above gave accurate a_N for 2,2,5,5-substituted pyrrolidine nitroxides, the calculated hfcc's for DMPO-O_2H using the same levels of theory gave hfcc's comparable to that predicted at B3LYP/6-31+G**//B3LYP/6-31G*. Hence, in this study, the a_N, $a_{\beta\text{-H}}$ and $a_{\gamma\text{-H}}$ for all of the spin adducts were only calculated at the B3LYP/6-31+G**//B3LYP/6-31G* level to show *qualitative* trends in the hfcc compared to the experimental.

Calculation of pK_a

In order to establish the final form of the DMPO-radical adducts in solution, the adduct and its corresponding conjugate acid (*i.e.,* DMPO-X^-/DMPO-XH, respectively) were theoretically optimized at the PCM/B3LYP/6-31+G**//B3LYP/6-31G* level. The free energies of proton dissociation were then used to approximate the acidity of the adducts based on our previous work, according to the relationship

$$pK_a = 0.538(\Delta G_{298K,aq}) - 136.9$$

derived from a list of similar compounds.[53]

EPR Measurements

EPR measurements were carried out on an X-band spectrometer with HS resonator at room temperature. General instrument settings are as follows unless otherwise noted: microwave power, 10 mW; modulation amplitude, 0.5 G; receiver gain $3.17–3.56 \times 10^5$, time constant, 82 ms, time sweep 42 s. The hyperfine splittings (hfcc) of the spin adducts were determined by simulating the spectra using the WinSim (NIEHS/NIH) package.[54] The relative intensity of each component of the spectra was also determined.

Spin Trapping Studies

DMPO, $Na_2S_2O_4$, Na_2SO_3, $(NH_4)_2S_2O_8$, all of high purity (>99.0%), H_2O (20% ^{17}O atom) and 80% H_2O_2 were all obtained commercially. All solutions were prepared using Dulbecco's phosphate buffered saline (Sigma). The total volume of each solution used for the EPR measurement was 50 μL, and was loaded into a 50 μL quartz micropipette. All samples had a 100 mM salt concentration in 100 mM DMPO in PBS. Sulfate radical anion and sulfur dioxide radical anion were generated from irradiation with a low-pressure mercury vapor lamp at 254 nm wavelength in aqueous solutions of 100 mM $(NH_4)_2S_2O_8$ or 100 mM $Na_2S_2O_4$ respectively.[10,16,55] Sulfite radical anion was generated following the same method as for the sulfate and sulfur dioxide radicals with the addition of H_2O_2 (0.2% in solution) in aqueous solution of 100 mM Na_2SO_3.[56] EPR spectra were acquired over the course of 10 min while the UV lamp was on.

RESULTS AND DISCUSSION

Sulfur Dioxide Radical Anion ($SO_2^{\bullet-}$) and Spin Adducts

Theoretical analysis of $SO_2^{\bullet-}$ carried out at the PCM/B3LYP/6-31G**//B3LYP/6-31G* level of theory is consistent with a bent geometry. The O-S-O bond angle deviates from the trigonal planar 119° of the non-radical SO_2 to 116.7° in the optimized structure of the radical anion. The charge density distribution of $SO_2^{\bullet-}$ from a natural population analysis reveals negative character on the two O atoms (−1.03 e) (Figure 1) and a positive charge on the S atom (1.05 e). Calculated S-O bond lengths in $SO_2^{\bullet-}$ gave a bond distance of 1.54 Å which are longer compared to the expected S-O double bond distances of 1.435 Å in SO_2[57] indicating that the S-Os are singly bonded in the radical anion form.

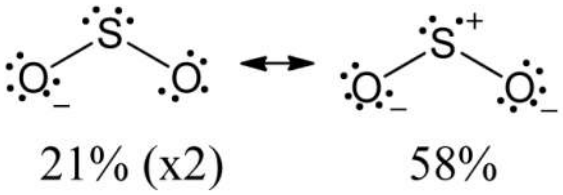

Natural population analysis also reveals a greater spin population density on S (0.58) than on the O atoms (0.21), indicating that the bond formed *via* radical addition will be between S and Cα of DMPO. This is confirmed by the energetics of formation for the radical anion addition to DMPO, in which the S-centered adduct ($\Delta G_{298K,aq}$ = 20.5 kcal/mol) is significantly less endoergic than the O-centered adduct ($\Delta G_{298K,aq}$ = 37.3 kcal/mol) (Figure S1), however in the $HSO_2^{\bullet}$ adduct formation, there was no significant difference in the energetics of formation between the S-centered adduct ($\Delta G_{298K,aq}$ = 14.9 kcal/mol) (Figure 2) and the O-centered adduct ($\Delta G_{298K,aq}$ = 15.0 kcal/mol) (Figure S1), perhaps due to the increased spin density on the unprotonated O in $HSO_2^{\bullet}$ (0.35) from the O atoms in the radical anion (0.21). Differences in charge on unprotonated O atoms in the radicals was not significant between the protonated and unprotonated forms (−0.82 e and −1.03 e respectively, Figure 1). Nevertheless, all sulfur dioxide radical adducts were calculated to be too endoergic to form in significant concentration, and only a singlet spectrum corresponding to $SO_2^{\bullet-}$ with no SO_2 spin adduct was detected by EPR in a solution of $Na_2S_2O_4$ (100 mM) and DMPO (100 mM) under 254 nm light, despite a slightly favorable free energy of formation calculated for the radical species:

$$S_2O_4^{2-} \overset{\Delta G_{298K,aq}=-7.7}{\rightleftharpoons} 2\,SO_2^{\bullet-}$$

Similar species such as chlorine dioxide radical ($ClO_2^{\bullet}$) and nitrogen dioxide radical ($NO_2^{\bullet}$) react readily with spin traps leading to the formation of oxygenated aminoxyl products, while $SO_2^{\bullet-}$ annihilates aminoxyl radical signals via reduction or addition and is known to be unreactive with spin traps.[17] Whereas $ClO_2^{\bullet}$, $NO_2^{\bullet}$ and $SO_2^{\bullet-}$ are all persistent radicals, reactions with spin traps vary greatly. On the other hand, the carbon dioxide anion radical $CO_2^{\bullet-}$ can readily form a spin adduct with DMPO.

Sulfur Trioxide Radical Anion ($SO_3^{\bullet-}$) and Spin Adducts

Theoretical analysis of $SO_3^{\bullet-}$ was carried out at the PCM/B3LYP/6-31G**//B3LYP/6-31G* level of theory and shows a trigonal pyramidal geometry. The charge density distribution of $SO_3^{\bullet-}$ from an NPA (Figure 1) reveals negative character on all three O atoms (−.99 e) and a positive charge on the S atom (1.97 e).

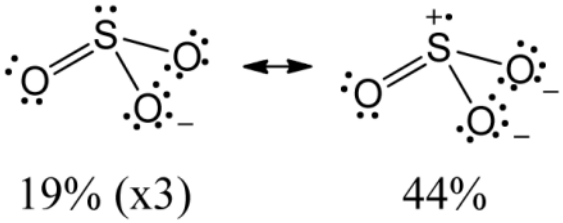

Additionally, the NPA reveals increased spin density distribution on the unprotonated O atoms of the bisulfite ($HSO_3^{\bullet}$) radical (0.24 and 0.26) versus the sulfite radical anion O atoms (0.19). Only the bisulfite radical adducts (both O- and S-centered) were calculated to

be significantly exoergic (DMPO$^{\bullet}$-OSO_2H $\Delta G_{298K,aq}$ = −11.3 kcal/mol, DMPO$^{\bullet}$-SO_3H $\Delta G_{298K,aq}$ = −3.1 kcal/mol, Figure 2). The formation of the sulfite radical adducts were calculated to be more endoergic (DMPO$^{\bullet}$-OSO_2^- $\Delta G_{298K,aq}$ = 3.2 kcal/mol, DMPO$^{\bullet}$-SO_3^- $\Delta G_{298K,\,aq}$ = 4.9 kcal/mol) than the formation of the bisulfite radical adducts. In spin trapping studies of aqueous sulfite/bisulfite (100 mM Na_2SO_3) and DMPO (100 mM) in 2.0% H_2O_2 under 254 nm light, a spin adduct was detected (Figure 3). Comparison of the hyperfine splitting constants taken from computer simulation of the experimental spectra (a_N = 14.5, $a_{H\text{-}\beta}$ = 16.1) qualitatively correlates best with the theoretical hyperfine splitting constants (Table 1) corresponding to DMPO$^{\bullet}$-SO_3H (a_N = 12.2, $a_{H\text{-}\beta}$= 14.1). In the calculated hfcc's of the DMPO-SO_3H radical adduct, the a_N is 1.87 G less than the $a_{H\text{-}\beta}$ compared to 1.59 G for our experimental sulfite radical adduct. All other calculated sulfite adducts exhibited the opposite trend (*i.e.,* $a_N > a_{H\text{-}\beta}$).

The determination that the adduct exists in the protonated S-centered form can be explained by the presence of a stabilizing intramolecular hydrogen bond yielding a pseudo-six-member ring in this structure (see section on adduct pK_a). The observed spectrum gradually decomposed to DMPO$^{\bullet}$-OH over the course of the experiment. Simulations of spectra taken at 0, 5, and 10 min showed increasing intensity for DMPO$^{\bullet}$-OH and decreasing sulfite/sulfate radical adduct concentrations as a function of time (Table 2). For the sake of thoroughness, we calculated the thermochemistries at the same level of theory for various conformers of a system consisting of a DMPO-bisulfite radical adduct with two water molecules and in consideration of the bulk dielectric effect of water. It was interesting to note that the most thermodynamically favourable structure did indeed break the intramolecular H-bond of the ring, however the next most favourable structure included the intramolecular H-bond of the intact ring and the difference in energy was only less than 7.5 kcal/mol leading us to believe that the ring conformer is a contributing structure and that these two forms may exist in equilibrium in solution. The intramolecular H-bond would needless to say contribute more in a less polar solvent. Perhaps more importantly, we found that the hyperfine coupling constants of the ring conformer still exhibited the qualitative trends that most closely matched our experimental data.

Sulfur Tetroxide Radical Anion ($SO_4^{\bullet -}$) and Spin Adducts

Theoretical analysis of $SO_4^{\bullet -}$ was carried out at the PCM/B3LYP/6-31G**//B3LYP/6-31G* level of theory and shows a tetrahedral geometry. Natural population analysis of the electronic structures of $SO_4^{\bullet -}$ and $HSO_4^{\bullet}$ reveal the S center is highly oxidized in both forms (2.52 e) and with negligible spin density (−0.06 and −0.07 respectively).

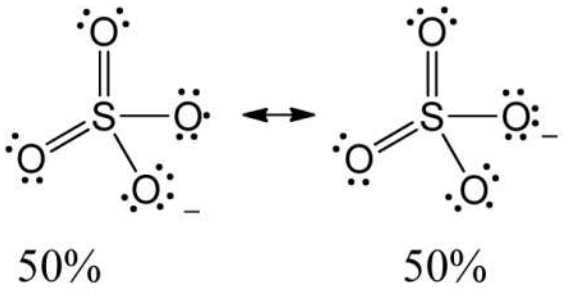

The only conceivable radical addition would yield an O-centered adduct, as the majority of the spin character is found to be distributed over two O atoms in both the sulfate and bisulfate radicals. The calculated free energies of adduct formation supports this reasoning: the S-centered adducts are calculated to be highly endoergic (DMPO$^{\bullet}$-SO_4^- $\Delta G_{298K,aq}$ = 105.8 kcal/mol, DMPO$^{\bullet}$-SO_4H $\Delta G_{298K,aq}$ = 77.7 kcal/mol) (Figure S1) while the O-

centered adducts are highly exoergic (DMPO•-OSO_3^- $\Delta G_{298K,\,aq}$ = −17.1 kcal/mol, DMPO•-OSO_3H $\Delta G_{298K,aq}$ = −28.9 kcal/mol) (Figure 2). The difference in energetics between the unprotonated and protonated O-centered adducts can be explained by the presence of a stabilizing intramolecular hydrogen bond in the protonated adduct (see section on adduct pK_a). In the spin trapping study of aqueous $(NH_4)_2S_2O_8$ (100 mM) and DMPO (100 mM) under 254 nm light, a signal was observed (Figure 3). Comparison of the hyperfine splitting constants taken from the computer simulation of the experimental spectra (a_N = 13.7, $a_{\beta\text{-H}}$ = 10.5, $a_{\gamma\text{-H}}$ = 1.5) qualitatively correlates best with the theoretical hyperfine splitting constants (Table 1) corresponding to DMPO•-OSO_3H (a_N = 11.4, $a_{\beta\text{-H}}$ = 8.9, $a_{\gamma\text{-H}}$ = 1.5). In the calculated hfcc's of DMPO-OSO_3H, the a_N was 2.55 G greater than the $a_{\beta\text{-H}}$ compared to 3.2 G for our experimental sulfate radical adduct. The DMPO•-OSO_3H adduct, like DMPO•-SO_3H was shown to gradually decompose to DMPO•-OH (Table 2) but at a relatively slower rate.

Acidity of Adducts

A pK_a value was calculated[53] for each DMPO•-SO_2H (both O- and S-centered), DMPO•-SO_3H (both O- and S-centered), and DMPO•-OSO_3H and the results are presented in Table 3. The pK_as of the DMPO•-SO_2H and DMPO•-OSOH adducts were calculated to be 5.9 and 13.2 respectively. The difference in acidity can be deduced from the adduct structures where the lack of resonance and charge delocalization in the conjugate base of the O-centered adduct is the likely cause of its high pK_a (Scheme 2). The structural assignments for the sulfite and sulfate radical adducts may prove puzzling as the experimentally observed hfcc's for the sulfur trioxide and sulfur tetroxide adducts were determined to be closer to the predicted hfcc's for DMPO•-SO_3H and DMPO•-OSO_3H respectively (Table 1). Yet, these adducts should be deprotonated at pH 7 as sulfonic acids (RSO_3H) and sulfate esters ($ROSO_3H$) are extremely acidic (pK_a Me-SO_3H = −1.92, pK_a Me-OSO_3H = −3.54)[58,59] and the calculated pK_a values for these species, although greater, are still highly acidic (Table 3). However, studying the structure of both adducts reveals that the acidic protons of both adducts are engaged in an intramolecular hydrogen bond with the nitronyl O atom, forming a pseudo-six-member ring in DMPO•-SO_3H, and a pseudo-seven-member ring in DMPO•-OSO_3H (Figure 4). Pseudo-five and six-member rings formed by intramolecular H-bonds have been long known to be uniquely stable structures that help stabilize a conjugate acid over its base form.[60] The inconsistency between the observed structure and the calculated pK_a can be rationalized by the fact that the calculation used to determine pK_a was developed as a method of approximation, and does not account for such intramolecular interactions. This idea may also help explain why the S-centered adduct was observed in the sulfite spin trapping experiment; the S-centered adduct results in a pseudo-six-member-ring, while an O-centered adduct would result in a less favorable pseudo-seven-member ring. It is also likely that despite the stabilizing geometry of the rings that the adducts would still exist in equilibrium with their conjugate bases and that the theoretical geometries assigned to these adducts resemble the most favorable approach-geometry of the bisulfite and bisulfate radicals to DMPO.

Mechanisms of Decomposition of $SO_3^{\bullet-}$ and $SO_4^{\bullet-}$ Adducts

Adducts of both sulfite and sulfate radical anions decomposed to DMPO•-OH and the possible mechanisms of decomposition were investigated. Although oxidation of DMPO by any present radicals to its radical cation form (DMPO$^{\bullet+}$) followed by hydration to form DMPO•-OH is possible, this mechanism is highly unlikely to occur based on [^{17}O] isotopic labeling experiments as previously discussed in detail by Mason and coworkers.[61,62] This suggests that nucleophilic substitution *via* hydrolysis is responsible for producing the hydroxyl radical adduct.[63] Two plausible mechanisms for the decomposition of the observed adducts to DMPO•-OH are hydrolysis at the C_α-O bond or O-S bond in O centered adducts

or the C_α-S bond in S-centered adducts (Scheme 3), or an intramolecular cleavage reaction (Scheme 4). Calculations were performed at the PCM/B3LYP/6-31G**//B3LYP/6-31G* level of theory for both mechanisms (Table 4). The results suggest that hydrolysis is most favorable, and thus responsible for most of the observed decomposition to DMPO$^\bullet$-OH.

Based on electrophilicity alone, nucleophilic attack of H_2O appears more likely to occur at the S atom than at the C_α in either adduct (DMPO$^\bullet$-SO_3H charge S = 2.34 e C_α = –0.32 e, DMPO$^\bullet$-OSO_3H charge S = 2.56 e C_α = 0.20 e). To confirm this hypothesis, an EPR experiment with DMPO, $(NH_4)_2S_2O_8$, and $H_2{}^{17}O$ was UV irradiated and yielded EPR spectrum. Figure 5 shows spectra with a multiplet EPR signal consistent with hfcc contribution from the ^{17}O isotope. Simulation of the spectra revealed hfcc's of a_N = 15.0–15.1, $a_{\beta\text{-H}}$ = 13.9-13.8, $a_{17\text{-O}}$ = 4.0 which can be assigned to the formation of DMPO$^\bullet$-^{17}OH. This data is consistent with those reported by Mason and coworkers for DMPO$^\bullet$-^{17}OH with hfcc values of a_N = 15.01, $a_{\beta\text{-H}}$ = 15.01, $a_{17\text{-O}}$ = 4.66. Figure 5a shows DMPO$^\bullet$-^{17}OH formation in the presence of $FeCl_3$ alone as control *via* metal-catalyzed Forrester-Hepburn mechanism, and Figure 5b shows a significant amount of DMPO$^\bullet$-^{17}OH (~ 12%) formed in the presence of irradiated $(NH_4)_2S_2O_8$. The formation of DMPO$^\bullet$-^{17}OH in Figure 5b suggests nucleophilic substitution by $H_2{}^{17}O$ occurs at the C_α in DMPO$^\bullet$-OSO_3H and predominates over the S-centered substitution in spite of the higher charge on the S atom compared to the C_α (Scheme 3). This suggests that sterics may be the more predominant factor over electrostatics in determining the mode of hydrolysis in O-centered adducts.

Examining the EPR spectra (Figure 3) from 0 minutes to10 minutes shows that the DMPO$^\bullet$-OSO_3H is more stable than the DMPO$^\bullet$-SO_3H. This stability for DMPO$^\bullet$-OSO_3H can be due to the fact that –OSO_3H group is bulkier than the –SO_3H group and thus presents a less favorable nucleophilic substitution reaction of H_2O. The intramolecular cleavage reaction on the other hand, is unaffected by steric factors as the first step is dissociative. The C_α-O bond of DMPO$^\bullet$-OSO_3H at 1.44Å is also shorter and hence stronger than the C_α-S bond of DMPO$^\bullet$-SO_3H at 1.86Å. The highly oxidized S atom of the –SO_3H group is also highly electron withdrawing (charge of S in DMPO$^\bullet$-SO_3H = 2.34 e), making it a much better leaving group than –OSO_3H (charge of O in DMPO$^\bullet$-OSO_3H = –0.75 e) in either an S_N1 or S_N2 type hydrolysis.

Nucleophilic Addition versus Radical Addition

Evidence regarding the Forrester-Hepburn adduct formation pathway is consistent with previous studies which have found it to be an unlikely source of the radical adducts.[62] Calculations were performed at the PCM/B3LYP/6-31G**//B3LYP/6-31G* level of theory for the mechanisms outlined in Table 5. Only the unprotonated sulfite adduct formation is thermodynamically feasible *via* the nucleophilic addition mechanism (DMPO-SO_3^- $\Delta G_{298K,aq}$ = 1.6, DMPO-OSO_2^- $\Delta G_{298K,aq}$ = −0.1) and while these values are slightly more exoergic than the equivalent radical addition mechanism (DMPO-SO_3^- $\Delta G_{298K,aq}$ = 4.9, DMPO-OSO_2^- $\Delta G_{298K,aq}$ = 3.2) it is noted that the addition of the bisulfite radical is more exoergic (DMPO-SO_3H $\Delta G_{298K,aq}$ = −3.1, DMPO-OSO_2H = −11.3) compared to the Forrester-Hepburn pathway in which the first step (i.e., nucleophilic addition of SO_3^{2-} to DMPO) is highly endoergic (DMPO-SO_3^{2-} $\Delta G_{298K,aq}$ = 36.2 kcal/mol, DMPO-OSO_2^{2-} $\Delta G_{298K,aq}$ = 36.0 kcal/mol) (Table 5).

CONCLUSIONS

Additions of $SO_2^{\bullet-}$, $SO_3^{\bullet-}$, and $SO_4^{\bullet-}$ to the spin trap DMPO were investigated experimentally using EPR and computationally at the PCM/B3LYP/6-31+G**//B3LYP/6-31G* level of theory. Spin trapping studies revealed signals for an S-centered sulfite radical adduct and an O-centered sulfate radical adduct, but no signal was observed for an

adduct of sulfur dioxide radical anion and DMPO. The spin trapping results were consistent with the computations that showed unfavorable addition for sulfur dioxide radical anion, a predominant S-centered adduct for $SO_3^{\bullet-}$, and a predominant O-centered adduct for $SO_4^{\bullet-}$. Both adducts were predicted to be protonated based on their optimized structures and qualitative comparison of the experimental and theoretical hfcc's. In the EPR study both adducts decomposed over time to DMPO$^{\bullet}$-OH, most likely *via* hydrolysis at the Cα as confirmed by ^{17}O isotope labeling of H_2O. An alternate, nucleophilic-addition mechanism to formation of the sulfite radical adduct (Forrester-Hepburn) was investigated at the PCM/B3LYP/6-31+G**//B3LYP/6-31G* level of theory and found to be unfavorable with respect to the radical addition mechanism.

Supplementary Material

Refer to Web version on PubMed Central for supplementary material.

Acknowledgments

This publication was made possible by Grant HL 81248 from the NIH National Heart, Lung, and Blood Institute. This work was supported in part by an allocation of computing time from the Ohio Supercomputer Center.

References

1. Gunnison AF, Jacobsen DW. Crit Rev Toxicol. 1987; 17:185.
2. Utell MJ, Marrow PE, Speers DM, Darling J, Hyde RW. Am Rev Respir Dis. 1983; 128:444. [PubMed: 6614638]
3. Pelltier M, Lavastre V, Girard D. Toxicol Sci. 2002; 69:210. [PubMed: 12215676]
4. Reist M, Marshall K, Jenner P, Halliwell B. J Neurochem. 1998; 71:2431. [PubMed: 9832141]
5. Thomas D, Yolande SK. Microbiol Mol Biol Rev. 1997; 61:503. [PubMed: 9409150]
6. Karakas E, Wilson HL, Graf TN, Xiang S, Jaramillo-Busquets S, Rajagopalan KV, Kisker C. J Biol Chem. 2005; 280:33506. [PubMed: 16048997]
7. Brown GK, Scholem RD, Croll HB, Wraith JE, McGill JJ. Neurology. 1989; 39:252. [PubMed: 2915798]
8. Shih VE, Abroms IF, Johnson JL, Carney M, Mandell R, Robb RM, Clotherty JP, Rajagopalan KV. N Engl J Med. 1977; 297:1022. [PubMed: 302914]
9. Ranguelova K, Chatterjee S, Ehrendhaft M, Ramirez DC, Summers FA, Kasiiska MB, Mason RP. Photochem Photobiol. 2010; 32:563.
10. Chignell CF, Kalyanaraman B, Mason RP, Sik RH. Photochem Photobiol. 1980; 32:563.
11. Mottley C, Mason RP, Chignell CF, Sivarajah K, Eling TE. J Biol Chem. 1982; 257:5050. [PubMed: 6279657]
12. Covello PS, Thompson JE. Biochem Biophys Acta, General Subjects. 1985; 843:150.
13. Shi X. J Inorg Biochem. 1994; 56:155. [PubMed: 7798899]
14. Alipazaga MV, Moreno RGM, Linares E, Medeiros MHG, Coichev N. J Chem Soc Dalton Trans. 2008:5636.
15. Niknahad H, O'Brien PJ. Chem-Biol Interact. 2008; 174:147. [PubMed: 18579106]
16. Neta P, Huie RE, Ross AB. J Phys Chem Ref Data. 1988; 17:1027.
17. Ohya-Nishiguchi, H.; Packer, L. Bioradicals Detected by ESR Spectroscopy. Birkhäuser: Basel; Boston; Berlin: 1995.
18. Ranguelova K, Mason RP. Free Radical Biol Med. 2009; 47:128. [PubMed: 19362142]
19. Elias RJ, Andersen ML, Skibsted LH, Waterhouse AL. J Agricul Food Chem. 2009; 57:4359.
20. Zalibera M, Rapta P, Stasko A, Brindzova L, Brezova V. Free Radical Res. 2009; 43:457. [PubMed: 19353392]
21. Potapenko DI, Bagryanskaya EG, Reznikov VV, Clanton TL, Khramtsov VV. Magn Reson Chem. 2003; 41:603.

22. Potapenko DI, Clanton TL, Bagryanskaya EG, Gritsan NP, Reznikov VA, Khramtsov VV. Free Radical Biol Med. 2003; 34:196. [PubMed: 12521601]
23. Villamena FA, Zweier JL. Antioxid Redox Signaling. 2004; 6:619.
24. Burgett RA, Bao X, Villamena FA. J Phys Chem A. 2008; 112
25. Locigno EJ, Zweier JL, Villamena FA. Org Biomol Chem. 2005; 3:3220. [PubMed: 16106305]
26. Villamena FA. J Phys Chem A. 2010; 114:1153. [PubMed: 19968309]
27. Villamena FA, Hadad CM, Zweier JL. J Phys Chem A. 2005; 109:1662. [PubMed: 16833491]
28. Villamena FA, Locigno EJ, Rockenbauer A, Hadad CM, Zweier JL. J Phys Chem A. 2006; 110:13253. [PubMed: 17149843]
29. Villamena FA, Locigno EJ, Rockenbauer A, Hadad CM, Zweier JL. J Phys Chem A. 2007; 111:384. [PubMed: 17214476]
30. Villamena FA, Merle JK, Hadad CM, Zweier JL. J Phys Chem A. 2007; 111:9995. [PubMed: 17845014]
31. Villamena FA, Xia S, Merle JK, Lauricella R, Tuccio B, Hadad CM, Zweier JL. J Am Chem Soc. 2007; 129:8177. [PubMed: 17564447]
32. Villamena FA, Das A, Nash KM. Future Med Chem. 2012; 4:1171. [PubMed: 22709256]
33. Floyd RA, Kopke RD, Choi CH, Foster SB, Doblas S, Towner RA. Free Radical Biol Med. 2008; 45:1361. [PubMed: 18793715]
34. Labanowski, JW.; Andzelm, J. Density Functional Methods in Chemistry. Springer; New York: 1991.
35. Parr, RG.; Yang, W. Density Functional Theory in Atoms and Molecules. Oxford University Press; New York: 1989.
36. Becke AD. Phys Rev. 1988; 38:3098.
37. Lee C, Yang W, Parr RG. Phys Rev B. 1988; 37:785.
38. Becke AD. J Chem Phys. 1993; 98:1372.
39. Hehre, WJ.; Radom, L.; Schleyer, PV.; Pople, JA. Ab Initio Molecular Orbital Theory. John Wiley & Sons; New York: 1986.
40. Tomasi J, Persico M. Chem Rev. 1994; 94:2027.
41. Cossi M, Barone V, Cammi R, Tomasi J. Chem Phys Lett. 1996; 255:327.
42. Barone V, Cossi M, Tomasi J. J Chem Phys. 1997; 107:3210.
43. Barone V, Cossi M, Tomasi J. J Comput Chem. 1998; 19:404.
44. Tomasi J, Mennucci B, Cammi R. Chem Rev. 2005; 105:2999. [PubMed: 16092826]
45. Frisch, MJ.; Trucks, GW.; Schlegel, HB.; Scuseria, GE.; Robb, MA.; Cheeseman, JR.; Scalmani, G.; Barone, V.; Mennucci, B.; Peterson, GA., et al. Revision A.01. Gaussian 09, Revision A.01. Gaussian, Inc; Pittsburgh PA: 2009.
46. Reed AE, Curtiss LA, Weinhold F. Chem Rev. 1988; 88:899.
47. Scott AP, Radom L. J Phys Chem. 1996; 100:16502.
48. Cirujeda J, Vidal-Gancedo J, Jurgens O, Mota F, Novoa JJ, Rovira C, Veciana J. J Am Chem Soc. 2000; 122:11393.
49. Pavone M, Cimino P, De Angelis F, Barone V. J Am Chem Soc. 2006; 128:4338. [PubMed: 16569010]
50. Saracino GAA, Tedeschi A, D'Errico G, Improta R, Franco L, Ruzzi M, Corvaia C, Barone V. J Phys Chem A. 2002; 106:10700.
51. Barone, V. Recent Advances in Density Functional Theory, Part 1. Cong, DP., editor. World Scientific Publishing Co; Singapore: 1995. p. 287
52. Woon DE, Dunning TH. J Chem Phys. 1995; 103:4572.
53. Villamena FA, Merle JK, Hadad CM, Zweier JL. J Phys Chem A. 2005; 109:6089. [PubMed: 16833946]
54. http://www.niehs.nih.gov/research/resources/software/tools/index.cfm.
55. Percec V, Popov AV, Ramirez-Castillo E, Coelho JFJ, Hinojosa-Falcon LA. J Polym Sci. 2004; 42:6267.

56. Ozawa T, Hanaki A. Biochem Biophys Res Commun. 1987; 142:410. [PubMed: 3028413]
57. Schomaker V, Stevenson DP. J Am Chem Soc. 1940; 62:1270.
58. Guthrie JP. Can J Chem. 1978; 56:2342.
59. Guthrie JP. J Am Chem Soc. 1980; 102:5177.
60. Silver BL, Luz Z, Peller S, Reuben J. J Phys Chem. 1966; 70:1434.
61. Mottley C, Connor HD, Mason RP. Biochem Biophys Res Commun. 1986; 141:622. [PubMed: 3026386]
62. Ranguelova K, Mason RP. Magn Reson Chem. 2011; 49:152. [PubMed: 21246623]
63. Davies MJ, Gilbert BC, Stell JK, Witwood AC. J Chem Soc Perkin Trans. 1992; 2:333.

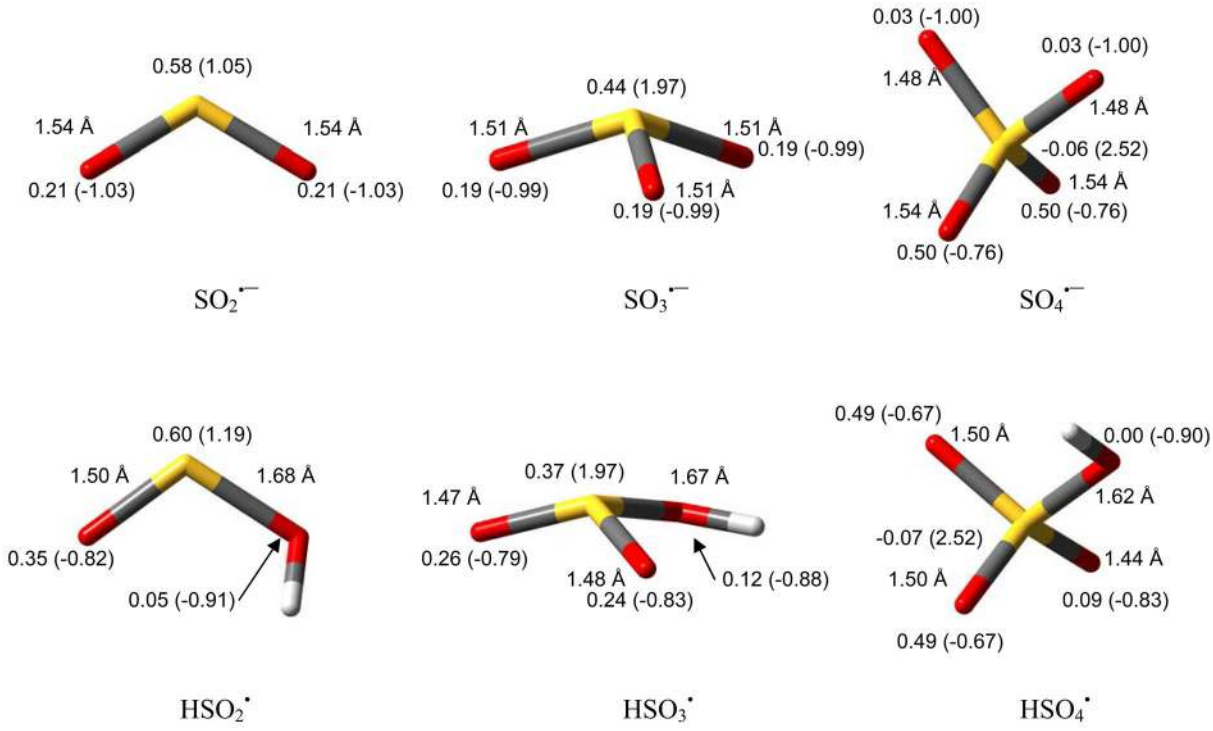

Figure 1.
Aqueous phase bond distances, spin and charge (in parentheses) densities of various radicals at the PCM/B3LYP/6-31+G**//B3LYP/6-31G* level.

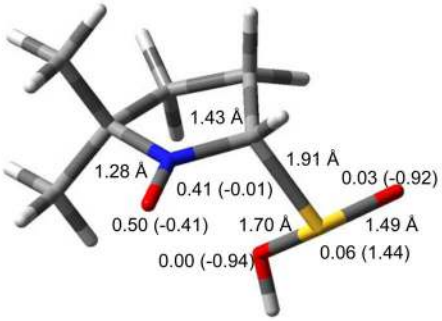

DMPO•-SO_2H
($\Delta G_{298K,aq} = 14.9$; $\Delta H_{298K,aq} = 10.2$)

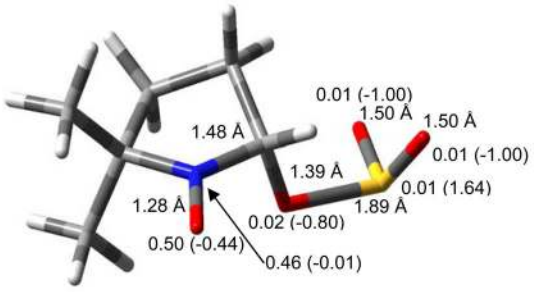

DMPO•-OSO_2^-
($\Delta G_{298K,aq} = 3.2$; $\Delta H_{298K,aq} = -12.6$)

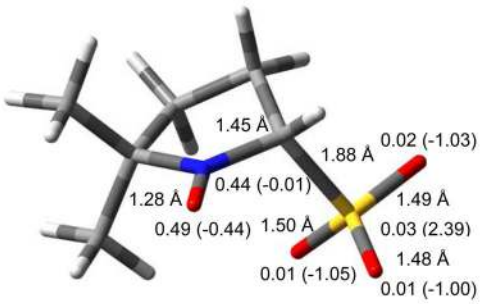

DMPO•-SO_3^-
($\Delta G_{298K,aq} = 4.9$; $\Delta H_{298K,aq} = -10.0$)

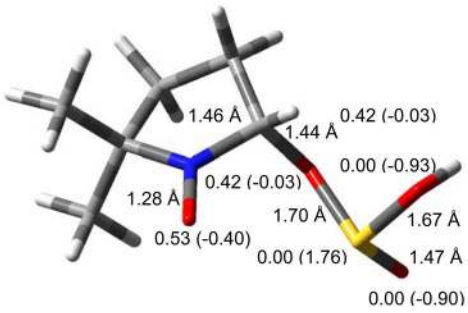

DMPO•-OSO_2H
($\Delta G_{298K,aq} = -11.3$; $\Delta H_{298K,aq} = -17.4$)

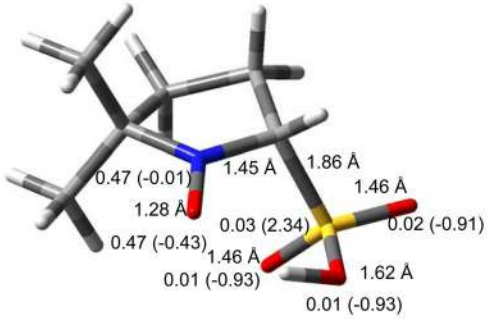

DMPO•-SO_3H
($\Delta G_{298K,aq} = -3.1$; $\Delta H_{298K,aq} = -12.4$)

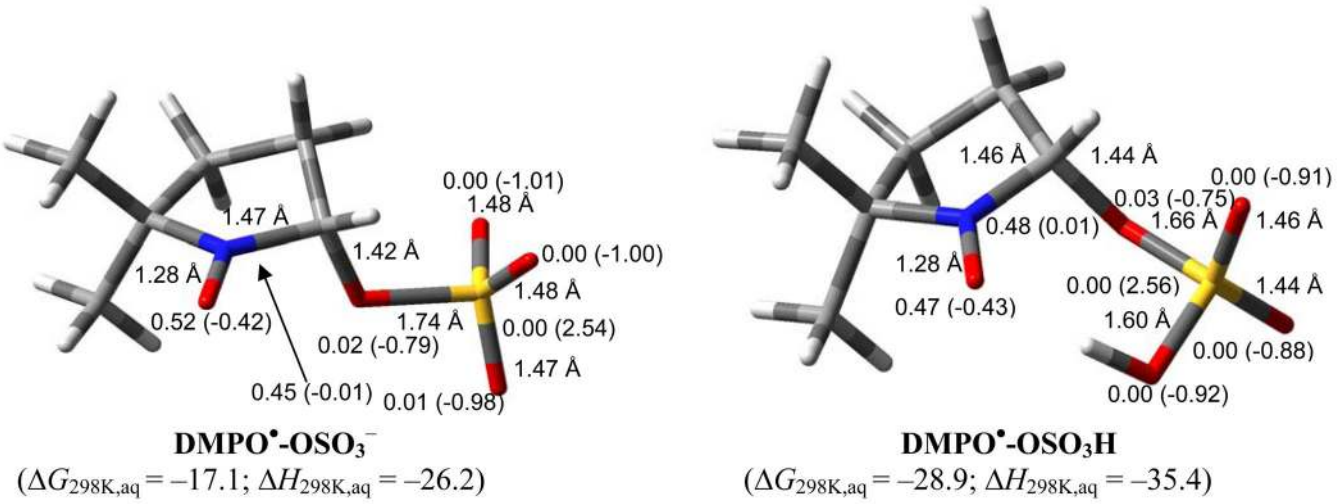

Figure 2.

Bond distances, spin and charge densities (in parentheses) of selected SO_2, SO_3, and SO_4 radical adducts of DMPO and their respective conjugate acids. Also shown are the aqueous phase free energies and enthalpies of reaction ($\Delta G_{298K,\,aq}$, $\Delta H_{298K,\,aq}$ in kcal/mol) at the PCM/B3LYP/6-31G**//B3LYP/6-31G* level of theory.

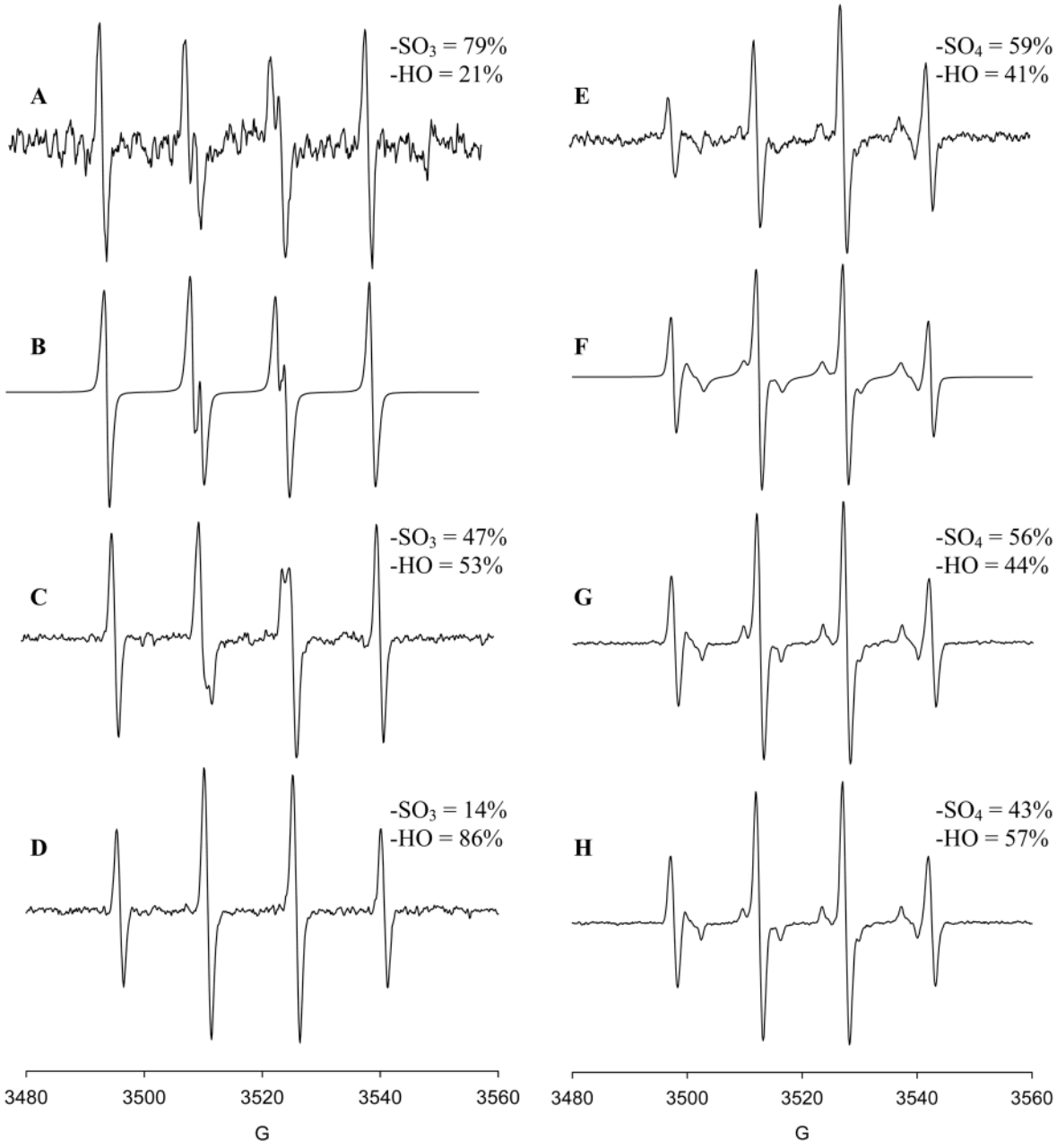

Figure 3.

X-band EPR spectra of DMPO (100 mM), Na_2SO_3 (100 mM) and H_2O_2 (2.0% v/v) under 254 nm light taken at (A) t = 0 min, (B) Simulation of A (DMPO$^{\bullet}$-SO_3: a_N = 14.52, $a_{\beta\text{-H}}$ = 16.11; DMPO$^{\bullet}$-OH: a_N = 15.02, $a_{\beta\text{-H}}$ = 14.50), (C) at t = 5 min, (D) at t = 10 min. Spectra of DMPO (100 mM) and $(NH_4)_2S_2O_8$ (100 mM) under 254 nm light taken at (E) t = 0 min, (F) Simulation of E (DMPO$^{\bullet}$-SO_4: a_N = 13.66, $a_{\beta\text{-H}}$ = 9.97, $a_{\gamma\text{-H1}}$ = 1.55, $a_{\gamma\text{-H2}}$ = 0.73; DMPO$^{\bullet}$-OH: a_N = 15.02, $a_{\beta\text{-H}}$ = 14.72), (G) at t = 5 min, (H) at t = 10 min.

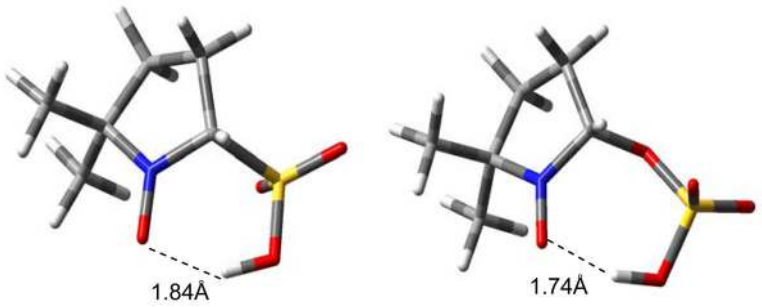

Figure 4.
Hydrogen bonding and the pseudo-ring formation of the optimized structures of DMPO•-SO_3H (left) and DMPO•-OSO_3H (right).

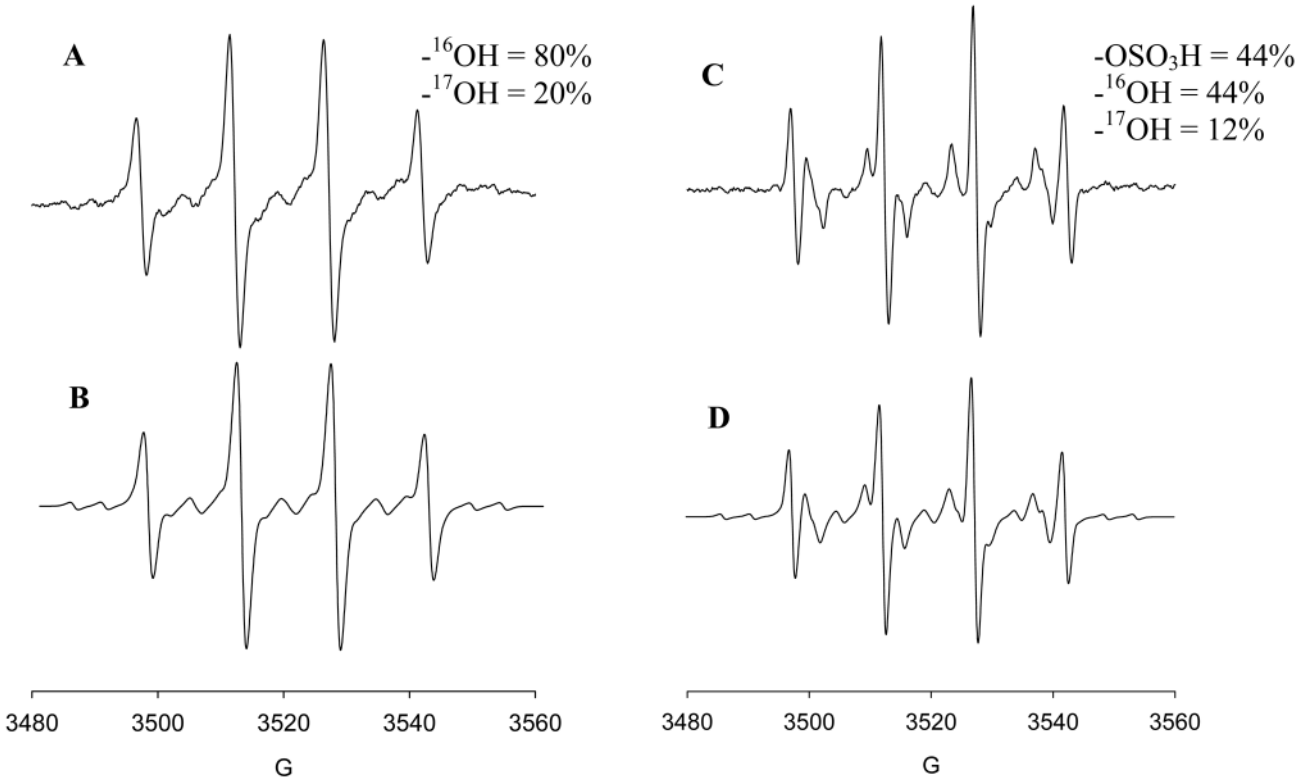

Figure 5.

(A) X-band EPR spectra of DMPO (100 mM), $FeCl_3$, and $H_2{}^{17}O$ (20% ^{17}O atom). (B) Simulation of A (DMPO$^{\bullet}$-^{16}OH: a_N = 14.96, $a_{\beta\text{-H}}$ = 14.68; DMPO$^{\bullet}$-^{17}OH: a_N = 15.11, $a_{\beta\text{-H}}$ = 13.93, $a_{17\text{-O}}$ = 4.81). (C) Spectra of DMPO (100 mM), $(NH_4)_2S_2O_8$, and $H_2{}^{17}O$. (D) Simulation of C (DMPO$^{\bullet}$-OSO_3H: a_N = 13.74, $a_{\beta\text{-H}}$ = 9.93, $a_{\gamma\text{-H1}}$ = 1.47, $a_{\gamma\text{-H2}}$ = 0.57; DMPO$^{\bullet}$-^{16}OH: a_N = 15.01, $a_{\beta\text{-H}}$ = 14.74; DMPO$^{\bullet}$-^{17}OH: a_N = 15.02,, $a_{\beta\text{-H}}$ = 13.84, $a_{17\text{-O}}$ = 4.84). Literature value for DMPO$^{\bullet}$-^{17}OH: a_N = 15.01, $a_{\beta\text{-H}}$ = 15.01, $a_{17\text{-O}}$ = 4.66.[62]

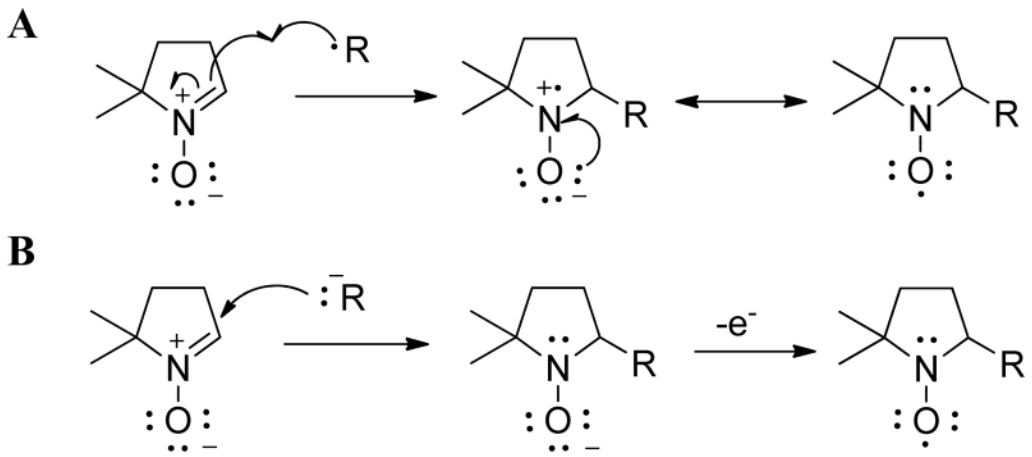

Scheme 1.
(A) Radical addition and (B) Forrester-Hepburn pathways for the formation of radical adduct

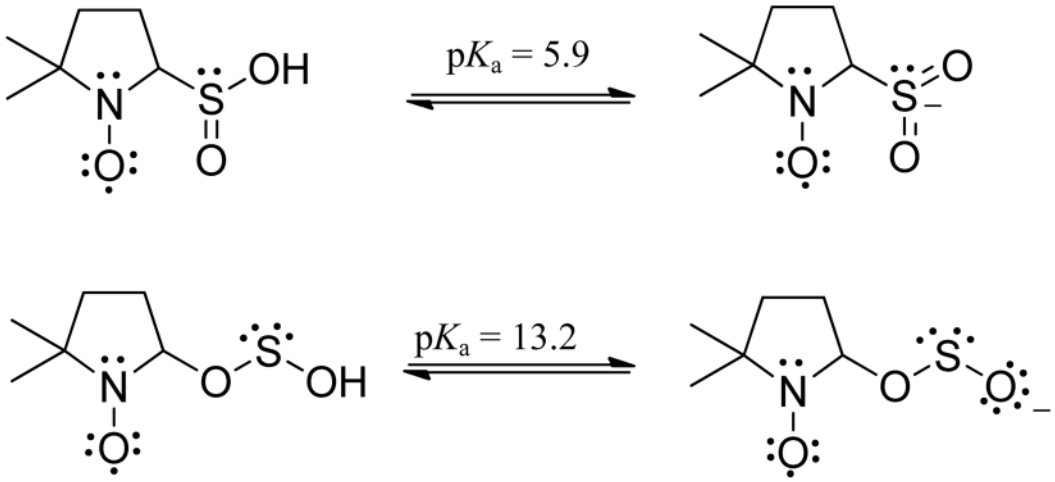

Scheme 2.
Acid-base chemistry of sulfur dioxide radical adducts

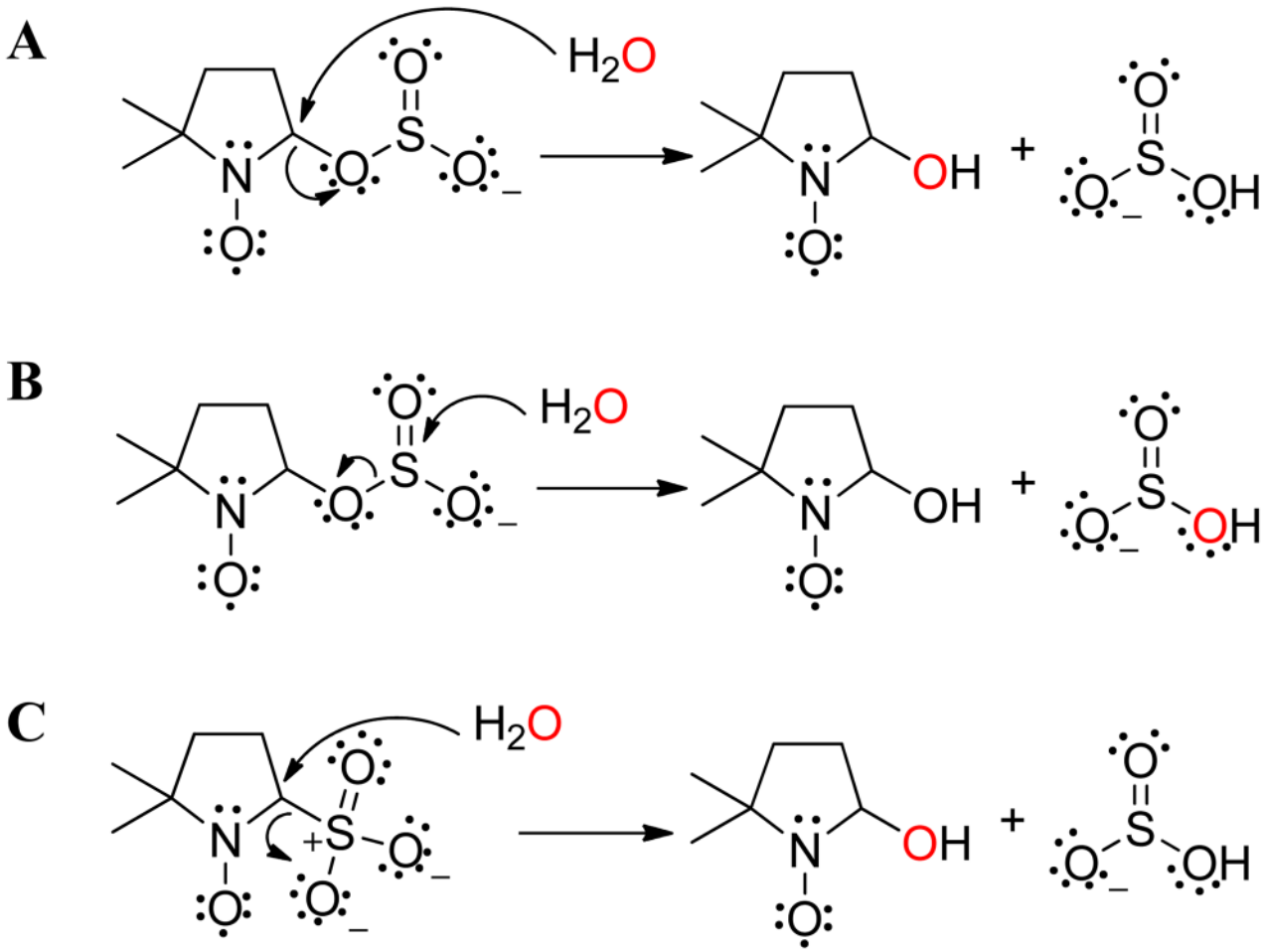

Scheme 3.

Hydrolysis of sulfite radical adduct showing nucleophilic substitution at the (A) Cα; (B) S; of the O-centered adducts as well as (C) Cα of the S-centered adduct. Only hydrolysis at Cα of an O-centered adduct will result in additional epr signal splitting in the presence of $^{17}OH_2$.

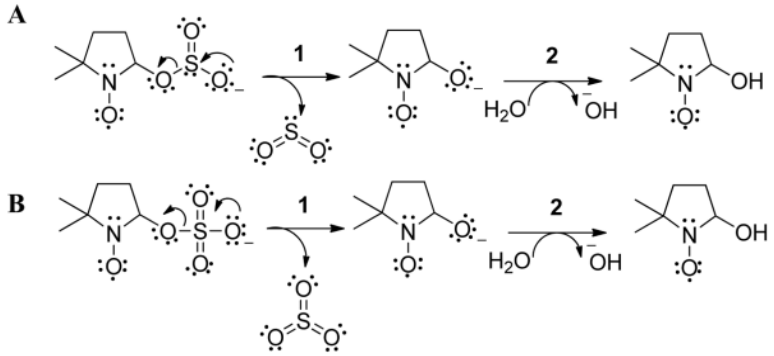

Scheme 4.
Intramolecular cleavage decomposition of (A) O-centered sulfite radical adducts; and (B) O-centered sulfate radical adduct

Table 1

Calculated hyperfine splitting constants (in Gauss, G) at the PCM/B3LYP/6-31G**//B3LYP/6-31G* level of theory and experimentally obtained hyperfine splitting constants.

adduct	isotropic hyperfine splitting constants (G)		
	Nitronyl-N	β-H	γ-H
theoretical			
DMPO•-OSO^-	10.8	6.1	2.3
DMPO•-OSOH	9.0	6.2	1.8
DMPO•-SO_2^-	11.7	18.8	1.9
DMPO•-SO_2H	9.4	13.8	1.3
DMPO•-OSO_2^-	12.1	3.8	1.2
DMPO•-OSO_2H	10.8	6.1	1.6
DMPO•-SO_3^-	11.0	9.4	1.0
DMPO•-SO_3H	12.2	14.1	1.6
DMPO•-OSO_3^-	11.0	4.2	1.7
DMPO•-OSO_3H	11.4	8.9	1.5
experimental			
DMPO•-SO_3^-	14.52	16.11	-
DMPO•-SO_4^-	13.66	10.46	1.53
DMPO•-OH	15.04	14.75	-
reported experimental[61,62]			
DMPO•-SO_3^-	14.7	15.9	
DMPO•-SO_4^-	13.8	10.1	1.38

Table 2

Relative areas of the sulfite and sulfate radical adducts with DMPO•-OH as a function of time

spin adduct prevalence		
scan time (min)	**DMPO•-SO_3**	**DMPO•-OH**
0	79%	21%
5	47%	53%
10	14%	86%
scan time (min)	DMPO•-SO_4	DMPO•-OH
0	59%	41%
5	56%	44%
10	43%	57%

Table 3

Calculated pK_a of the conjugate acids of various adducts

DMPO•-X	pK_a
-OSOH	13.2
-SO_2H	5.9
-OSO_2H	3.6
-SO_3H	0.9
-OSO_3H	−1.3

Table 4

Thermochemistries (in kcal/mol) of the various decomposition pathways at the PCM/B3LYP/6-31G**// B3LYP/6-31G* level of theory.

hydrolysis

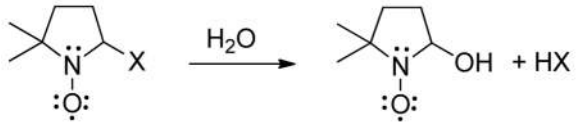

DMPO•-X + H_2O	**DMPO•-OH + HX**	**$\Delta G_{298K,aq}$**	**$\Delta H_{298K,aq}$**
DMPO•-SO_3^-	HSO_3^-	−3.5	7.2
DMPO•-OSO_2^-	HSO_3^-	−1.8	9.8
DMPO•-OSO_3^-	HSO_4^-	−2.6	3.9

intramolecular cleavage

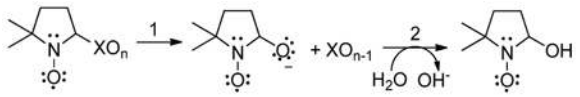

1

DMPO•-OX_n	**DMPO•-O^- + XO_{n-1}**	$\Delta G_{298K,aq}$	$\Delta H_{298K,aq}$
DMPO•-OSO_2^-	SO_2	16.9	29.8
DMPO•-OSO_3^-	SO_3	48.8	62.4

2

		$\Delta G_{298K,aq}$	$\Delta H_{298K,aq}$
DMPO•-O^-, H_2O	**DMPO•-OH, OH^-**	5.4	59.0

net intramolecular cleavage energetics

Adduct	$\Delta G_{298K,aq}$	$\Delta H_{298K,aq}$
DMPO•-OSO_2^-	22.4	88.8
DMPO•-OSO_3^-	57.2	121.4

Table 5

Thermochemistries (in kcal/mol) of the Forrester-Hepburn-mediated spin adduct formation at the PCM/B3LYP/6-31G**//B3LYP/6-31G* level of theory.

free energies and enthalpies of reaction (kcal/mol)

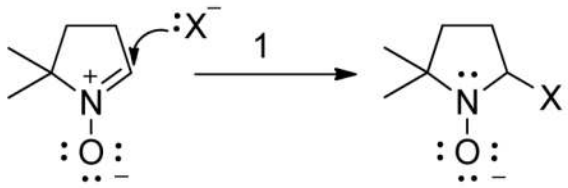

Anion (X)	Products (DMPO⁻-X)	$\Delta G_{298K,aq}$	$\Delta H_{298K,aq}$
SO_3^{2-}	DMPO⁻-SO_3^-	36.3	−37.9
SO_3^{2-}	DMPO⁻-OSO_2^-	36.0	−41.4
HSO_3^-	DMPO⁻-SO_3H	13.4	−6.5
HSO_3^-	DMPO⁻-OSO_2H	10.7	−4.8

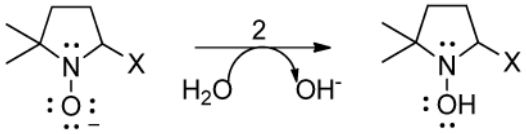

DMPO⁻-X	Protonated nitrone (DMPOH-X)	$\Delta G_{298K,aq}$	$\Delta H_{298K,aq}$
DMPO⁻-SO_3^-	DMPOH-SO_3^-	−2.7	−40.0
DMPO⁻-OSO_2^-	DMPOH-OSO_2^-	−5.8	−38.9
DMPO⁻-SO_3H	DMPOH-SO_3H	52.4	110.6
DMPO⁻-OSO_2H	DMPOH-OSO_2H	47.4	98.1

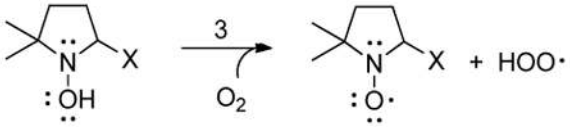

DMPOH-X	Radical adduct (DMPO•-X)	$\Delta G_{298K,aq}$	$\Delta H_{298K,aq}$
DMPOH-SO_3^-	DMPO•-SO_3^-	−31.9	−21.9
DMPOH-OSO_2^-	DMPO•-OSO_2^-	−30.3	−22.0
DMPOH-SO_3H	DMPO•-SO_3H	−30.6	−27.4
DMPOH-OSO_2H	DMPO•-OSO_2H	−31.0	−21.6

Overall energetics for the Forrester-Hepburn Mechanism (sum of steps 1–3)

Radical adduct	$\Delta G_{298K,aq}$	$\Delta H_{298K,aq}$
DMPO•-SO_3^-	1.6	−99.8
DMPO•-OSO_2^-	−0.1	−102.4

free energies and enthalpies of reaction (kcal/mol)

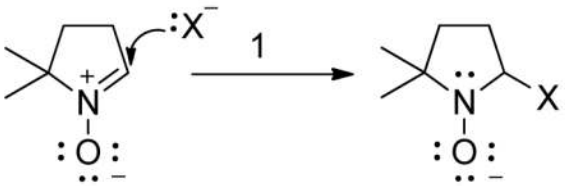

Anion (X)	Products ($DMPO^{-}$-X)	$\Delta G_{298K,aq}$	$\Delta H_{298K,aq}$
$DMPO^{\bullet}$-SO_3H		35.2	76.6
$DMPO^{\bullet}$-OSO_2H		27.1	71.6